

1           **The changing character of twenty-first century precipitation over the**  
2           **western United States in the variable-resolution CESM**

3           Xingying Huang, \* Paul A. Ullrich

4           *Department of Land, Air and Water Resources, University of California, Davis*

5           \*Corresponding author address: Xingying Huang, Department of Land, Air and Water Resources,  
6           University of California Davis, Davis, CA 95616.  
7           E-mail: xyhuang@ucdavis.edu

## ABSTRACT

8 (To be added once the main content settled down)

9     **1. Introduction**

10    There is substantial and growing interest in understanding the character of precipitation within  
11    a changing climate, in large part because of the pronounced impacts of water availability on  
12    socioeconomic and natural systems (Hegerl et al. 2004; Kharin et al. 2007; Scoccimarro et al.  
13    2013). Among these studies, precipitation extremes have been a major focus, particularly drought  
14    and flood events (Seneviratne et al. 2012). Studies examining the character of precipitation in a  
15    warming world, which utilize models of varying complexity from simple thermodynamic models  
16    through complex coupled climate simulations, suggest that although atmospheric water vapor is  
17    increasing, the consequences for precipitation are far more complicated. Extreme precipitation  
18    events are particularly nuanced: Our best projections suggest that extreme precipitation events  
19    will intensify even in regions where mean precipitation decreases (Tebaldi et al. 2006; Kharin  
20    et al. 2007).

21    Although future climate projections are subject to large uncertainties, climate models are  
22    nonetheless one of the most versatile tools for studying climate variability and extremes events  
23    in the future (Easterling et al. 2000). Global climate models (GCMs) have often been used to  
24    investigate changes in the mean, variability and extremes of climate, as forced with predicted  
25    greenhouse gas (GHGs) concentrations and aerosol emissions (Meehl et al. 2006). Several past  
26    studies have investigated global impacts (Seneviratne et al. 2012), but studies addressing impacts  
27    at local and regional scales are less common. Although increased GHG concentrations have con-  
28    tributed to the observed intensification of heavy precipitation events over the tropical ocean (Allan  
29    and Soden 2008) and the majority of Northern Hemisphere overland areas Min et al. (2011), these  
30    impacts are much more poorly understood at regional scales due to variability at finer spatial scales  
31    associated with the atmospheric circulation (Trenberth 2011). As a consequence of this variability,

<sup>32</sup> a confident assessment of changes in regional extremes requires both high spatial resolution and a  
<sup>33</sup> long integration period.

<sup>34</sup> Insufficient regional-scale climate information has been a major outstanding problem in climate  
<sup>35</sup> science, as stakeholders and water managers typically require fine-scale information on climate  
<sup>36</sup> impacts in order to effectively develop adaptation and mitigation strategies. In order to reach the  
<sup>37</sup> scales needed for effective local planning, dynamical downscaling with regional climate models  
<sup>38</sup> (RCMs) has been typically used to ascertain the frequency, intensity, and duration of extreme  
<sup>39</sup> events. By only simulating a limited regional domain, RCMs better capture fine-scale dynami-  
<sup>40</sup> cal features under high horizontal resolution (Bell et al. 2004; Frei et al. 2006; Rauscher et al.  
<sup>41</sup> 2010; Wehner 2013). Higher resolution can also enable more accurate simulation of precipitation  
<sup>42</sup> extremes, which can be driven by land use, land/water contrast, snow cover, cloudiness and circu-  
<sup>43</sup> lation patterns associated with topography (Leung et al. 2003a; Diffenbaugh et al. 2005; Salathé Jr  
<sup>44</sup> et al. 2008; Wehner et al. 2010). Diffenbaugh et al. (2005) studied both heat events and wet events  
<sup>45</sup> over the contiguous United States based on RCMs simulation at 25 km horizontal resolution, and  
<sup>46</sup> demonstrated that fine-scale processes were critical for accurate assessment of local- and regional-  
<sup>47</sup> scale climate change vulnerability. Leung et al. (2003b) showed that the higher-resolution RCMs  
<sup>48</sup> yield more realistic precipitation patterns and produce more frequent heavy precipitation over the  
<sup>49</sup> western U.S. (WUS), consistent with observations.

<sup>50</sup> Despite their success, RCMs also have known issues associated with inconsistency between the  
<sup>51</sup> lateral forcing data and the driven RCM, and the menu of physical parameterizations and param-  
<sup>52</sup> eters typically available to RCMs can lead to over-tuning of the model for a particular geographic  
<sup>53</sup> region or climatological field (McDonald 2003; Laprise et al. 2008; Mesinger and Veljovic 2013).  
<sup>54</sup> Consequently, there has been growing interest in variable-resolution enabled GCMs (VRGCMs)  
<sup>55</sup> to improve regional climate simulations. Unlike RCMs, which require GCM data to drive the sim-

ulation at lateral boundaries, VRGCMs use a unified model with coarse global resolution and enhanced resolution over a specific study region (Staniforth and Mitchell 1978; Fox-Rabinovitz et al. 1997). VRGCMs have demonstrated comparable utility for regional climate studies at a reduced computational cost, particular when compared to uniform-resolution GCMs (Fox-Rabinovitz et al. 2006; Rauscher et al. 2013).

In this paper, we utilize the recently developed variable-resolution option in the Community Earth System Model (VR-CESM). VR-CESM is based on the CESM (and its predecessor, the Community Climate System Model (CCSM)), a family of models that have been used for decades to study the global climate (Neale et al. 2010a; Hurrell et al. 2013). The overall performance of VR-CESM for modeling regional climate in the California and Nevada is detailed in Huang et al. (2016), where it was argued that VR-CESM has competitive biases in comparison to the Weather Research and Forecasting (WRF) model (a traditional RCM) and the uniform-resolution CESM, when evaluating both against high-quality observations and reanalysis. VR-CESM has been used in a number of studies to capture fine-scale atmospheric processes (Zarzycki et al. 2014, 2015; Rhoades et al. 2015). It was also shown that VR-CESM did not suffer from apparent artifacts within the coarse-fine transition region.

This study focuses on changes in the character of precipitation over the 21st Century within the WUS, as predicted from long-term ensemble runs conducted with VR-CESM with a local grid resolution of  $\sim 0.25^\circ$ . The WUS is known to be particularly vulnerable to hydrological extreme events, particularly floods and droughts (Leung et al. 2003b; Caldwell 2010), and hosts a variety of local features and microclimates associated with its rough and varied topography. Simulations of the future climate are performed in accordance with the representative concentration pathway (RCP) 8.5 scenario, which describes a “business-as-usual” projection for GHGs (Riahi et al. 2011). RCP8.5 is a baseline scenario with updated base year calibration (to 2005) and no

80 explicit climate policy. In this study we focus on a single RCP since end-of-century projections  
81 with the substantially more optimistic RCP2.6 scenario have been found to be qualitatively sim-  
82 ilar to mid-century RCP8.5 results (which are assessed in this study). Simulations are further  
83 conducted in accordance with the Atmospheric Model Intercomparison Project (AMIP) protocol  
84 (Gates 1992), a widely-used approach for climate model diagnosis, validation and intercompari-  
85 son that imposes global sea surface temperatures (SSTs) and sea ice. By constraining atmospheric  
86 boundary conditions at the sea surface, we avoid model biases that are known to exist in the fully  
87 coupled configuration (Grodsky et al. 2012; Small et al. 2014) and accept potential uncertainties  
88 associated with our choice of SSTs.

89 Changes in the character of precipitation, in terms of frequency and intensity, have been assessed  
90 in our study from recent history through the end of 21st century. A comprehensive set of metrics  
91 for precipitation extremes have been evaluated from ensemble simulations over the 26-year peri-  
92 ods corresponding to historical (1980-2005), mid-century (2025-2050) and end-of-century (2075-  
93 2100). We hypothesize that spatial inhomogeneity in local geography and temperature will also  
94 result in similarly inhomogeneous impacts on the precipitation field. We expect that teleconnec-  
95 tions (specifically the El Niño-Southern Oscillation, ENSO) will have a pronounced impact on  
96 precipitation features over particular area under the changes of mean SST and its variations. Since  
97 only one SST dataset was used for this study, we note that our projections are conditioned on a  
98 particular future character of ENSO. This is a potentially large source of uncertainty, as at present  
99 there is no clear consensus on how ENSO may behave under a warming climate (Fedorov and  
100 Philander 2000; Guilyardi et al. 2009), and strengthening or weakening of this pattern will have  
101 clear consequences for our results.

102 This work builds on a number of previous studies that have explored the projected future change  
103 in WUS precipitation. For example, Kim (2005) applied downscaled climate change signals to se-

104 lected indicators, and concluded that global warming induced by increased CO<sub>2</sub> is likely to drive  
105 increases in extreme hydrologic events in the WUS. Duffy et al. (2006) found that mean precip-  
106 itation predicted by the RCMs are not statistically significant compared to interannual variability  
107 in many regions over WUS, although there is little consistency among the different RCMs as to  
108 responses in precipitation to increased GHGs. Gao et al. (2015) pointed out a potentially large  
109 increase in atmospheric river events by the end of the 21st century under the RCP8.5 scenario.

110 This paper is structured as follows. Section 2 describes the model setup. Section 3 describes  
111 the methodology and reference datasets employed. An assessment of the ability of the model to  
112 capture the climatology of the WUS is given in section 4. Results from the future mean climato-  
113 logical trend and projected changes to precipitation indices are in section 6. Section 7 summarizes  
114 the main points of the study along with further discussion.

## 115 2. Model Setup

116 CESM is a state-of-the-art Earth modeling framework, consisting of coupled atmosphere, ocean,  
117 land and sea ice models (Neale et al. 2010b; Hurrell et al. 2013). In this study, Community At-  
118 mosphere Model version 5 (CAM5) (Neale et al. 2010b) and the Community Land Model version  
119 4.0 (Oleson et al. 2010) are used. Within CAM5, we use the Spectral Element (SE) dynamical  
120 core, which incorporates the variable-resolution option (Zarzycki et al. 2014) and includes de-  
121 sirable conservation and parallel scalability properties (Dennis et al. 2011; Taylor 2011). CLM  
122 is employed in the *unigrid* configuration, which allows the land model to be co-located with the  
123 atmospheric grid and so eliminates the need for interpolation. SSTs and sea ice, which are used  
124 to compute ocean-atmosphere fluxes, are prescribed in accordance with the AMIP protocol (Gates  
125 1992). The variable-resolution mesh used for this study is depicted in Figure 1, in accord with our  
126 past studies (Rhoades et al. 2015; Huang et al. 2016; Huang and Ullrich 2016).

127 Simulations have been performed for the historical period (1979-2005, hereafter referred to as  
128 `hist`) and for two future periods: 2024-2050 (hereafter referred to as `mid`) and 2074-2100 (hereafter  
129 referred to as `end`). For purposes of analysis, the first year of each time period was discarded as a  
130 spin-up period to allow adequate time for the initialized land and atmosphere to equilibrate. The  
131 26-year duration was chosen to provide an adequate sampling of annual variability for each time  
132 phase. For future projections, GHG concentrations are set based on RCP8.5. Historical SSTs and  
133 sea ice are prescribed at  $1^{\circ}$  resolution, as described by Hurrell et al. (2008). SSTs and sea ice  
134 for each future period are developed from fully-coupled RCP 8.5 climate simulations with bias  
135 correction applied (Cecile Hannay, personal communication). Using prescribed SSTs in place of  
136 a coupled ocean model considerably reduces the computation cost and so allows the atmospheric  
137 model to be run at a higher overall resolution. Annually-updated land surface datasets, which  
138 prescribe land-use characteristics, are interpolated from  $0.5^{\circ}$  to the land model grid.

139 Ensemble runs are needed to ensure that the sample adequately accounts for climate variability,  
140 especially for statistics associated with climatological extremes. However, the exact number of  
141 ensemble members required is heavily dependent on the variability of the particular metric being  
142 examined, and so no standard ensemble criteria exists (Deser et al. 2012b). Deser et al. (2012b)  
143 suggest that around 3 ensemble runs are required to detect a significant epoch difference for JJA  
144 (June-July-August) surface temperatures, whereas 10 to 30 ensemble members are needed for that  
145 for DJF (Dec.-Jan.-Feb.) precipitation. In our study, the use of prescribed SSTs does reduce the  
146 intrinsic variability of the climate system (see supplement), and so we found reasonably converged  
147 results with two ensemble members for the historical period and four ensemble members for each  
148 future period.

<sup>149</sup> **3. Methodology**

<sup>150</sup> *a. Precipitation indices*

<sup>151</sup> In order to fully account for the precipitation distributions, daily output over all the years are  
<sup>152</sup> utilized in data analysis. We have employed standard indices to characterize precipitation (Tebaldi  
<sup>153</sup> et al. 2006; Zhang et al. 2011; Sillmann et al. 2013). Several indices have been examined, including  
<sup>154</sup> those defined by the Expert Team on Climate Change Detection and Indices (ETCCDI) (Karl  
<sup>155</sup> et al. 1999) that have been primarily adopted in previous studies (Dulière et al. 2011; Sillmann  
<sup>156</sup> et al. 2013; Diffenbaugh et al. 2005; Singh et al. 2013) and others such as return levels, dry spell  
<sup>157</sup> and wet spell defined by either percentiles or by selected thresholds. As a result, loosely based  
<sup>158</sup> on the former studies, the indices we have chosen for this study attempt to provide a relatively  
<sup>159</sup> comprehensive characterization of precipitation, along with being easy to interpret and relevant to  
<sup>160</sup> stakeholders. The indices employed are summarized in Table 1.

<sup>161</sup> *b. Impacts of ENSO*

<sup>162</sup> The impact of ENSO on precipitation is emphasized in our study due to its influence on pre-  
<sup>163</sup> cipitation over a majority of our study area, particularly in the southwest U.S. (Cayan et al. 1999;  
<sup>164</sup> Zhang et al. 2010; Deser et al. 2012a; Yoon et al. 2015). The phase of ENSO (*i.e.* El Niño and La  
<sup>165</sup> Niña) is identified each year using the Oceanic Niño Index (ONI), defined as the 3-month running  
<sup>166</sup> means of SST anomalies in the Niño 3.4 region (covering 5N-5S, 120-170W based on NOAA  
<sup>167</sup> (2013)). An El Niño or La Niña episode is said to occur when the ONI exceeds +0.5 or -0.5  
<sup>168</sup> for at least five consecutive months for a water year (*i.e.* from July to June) (NOAA 2013) (see  
<sup>169</sup> the supplement). In order to remove the trend in the SST field associated with climate change,  
<sup>170</sup> the anomaly is computed against the detrended mean SSTs from the periods 1971-2000, 2020-

171 2050 and 2070-2100 for hist, mid and end respectively, using the aforementioned observed and  
172 predicted SST datasets. As argued by Kao and Yu (2009), an extended Niño 3.4 region may be  
173 necessary to determine the phase of ENSO – to determine if this was the case, SST anomalies  
174 were integrated over the region 105-170W, but it was observed that this had no significant impact  
175 on ONI statistics.

176 Student's t-test has been used to test whether or not two datasets at each grid point are statis-  
177 tically equivalent, if the sample population can be adequately described by a normal distribution.  
178 The normality of a dataset is assessed under the Anderson-Darling test. When the sample popu-  
179 lations do not approximately follow a normal distribution, Mann-Whitney-Wilcoxon (MWW) test  
180 is employed in lieu of the t-test. All these tests are evaluated at the 0.05 ( $\alpha$ ) significance level.  
181 Among different time periods, those statistical tests are conducted using all the yearly values of  
182 each ensemble run.

183 (add description of the supplement like what are included; see the `sst_enso.pdf`, mask the land  
184 (over land, it should the surface temperature.))

185 *c. Reference datasets*

186 Gridded observational datasets and reanalysis of the highest available quality with comparable  
187 horizontal resolutions to our VR-CESM simulations are used for assessing the simulation qual-  
188 ity. The use of multiple reference datasets is necessary due to the underlying uncertainty in the  
189 reference data. Descriptions of the datasets employed are as follows.

190 **UW Precipitation Dataset:** The UW daily gridded meteorological data is obtained from the  
191 Surface Water Modeling group at the University of Washington (Maurer et al. 2002; Hamlet  
192 and Lettenmaier 2005). UW incorporates topographic corrections for the precipitation. The  
193 dataset is provided at  $0.125^\circ$  horizontal resolution covering the period 1949 to 2010.

194       **NCEP CPC:** This dataset provides gauge-based analysis of daily precipitation from the Na-  
195       tional Oceanic and Atmospheric Administration (NOAA) Climate Prediction Center (CPC).  
196       It is a suite of unified precipitation products obtained by combining all information avail-  
197       able at CPC via the optimal interpolation objective analysis technique. The gauge analysis  
198       covers the Conterminous United States with a fine-resolution at  $0.25^{\circ}$  from 1948-01-01 to  
199       2006-12-31.

200       **North American Regional Reanalysis (NARR):** The is the NCEP (National Centers for En-  
201       vironmental Prediction) high-resolution reanalysis product that provides dynamically down-  
202       scaled data over North America at  $\sim 32$  km resolution and 3-hourly intervals from 1979  
203       through present (Mesinger et al. 2006).

## 204       4. Model Assessment

205       Before proceeding, we first investigate how well the model is able to represent the character  
206       of precipitation over the WUS. Figures 2 and Figure 3 depict the spatial character of the indices  
207       defined in Table 1. Considering the uncertainty within the reference datasets, the mean of the ref-  
208       erences are used to get the difference from the model output. T-test is applied here with UW, CPC  
209       and NARR as the three statistical samples and the historical runs as two samples averaged over  
210       the whole period, determining at each spatial point whether VR-CESM is statistically equivalent  
211       to the references as stippled in 2 and 3.

212       Compared with observations, VR-CESM well represents the spatial pattern of precipitation, with  
213       majority of the precipitation distributed along the northwest coastal area and the mountainous re-  
214       gions of the Cascades and the Sierra Nevada. Compared to the mean of the references, VR-CESM  
215       does overestimate the Pr significantly over most of the relatively dry region for about 0.2 mm to  
216       1.5 mm, especially over the eastern side of the Cascades and both sides of the Sierra Nevada (with

217 relatively difference reaching 50%-150%). This is further reflected in the overestimation of the  
218 non-extreme Pr events frequency (with  $\text{Pr} < 10 \text{ mm/day}$ ) since most precipitation over dry area  
219 is associated with low rainy rate days. However, for the western flank of the Sierra Nevada, the  
220 overestimation of the mean Pr is mainly due to the intensified rain rate, which may related with  
221 the strengthened treatment of orographic effects with excessively strong upward winds. Nonethe-  
222 less, the model captures the precipitation features including frequency and intensity satisfactorily  
223 over the main wet region, where most precipitation is resulted from extreme Pr events (when  
224  $\text{Pr} > 10 \text{ mm/day}$ ), without significant difference.

225 The corresponding contribution fraction to total precipitation amount of each range defined in  
226 our metrics is also well represented in the model without significant difference, except the western  
227 side of the the Sierra Nevada and eastern flank of the Cascades in the Washington. This suggests  
228 that despite the aforementioned biases, VR-CESM can still capture the overall shape of the precip-  
229 itation distributions. Biases in simulating extreme precipitation over the topographically complex  
230 regions including the Cascades and Sierra Nevada ranges have also been found by in the high-  
231 resolution simulation by RCMs Walker and Diffenbaugh (2009); Singh et al. (2013), and have  
232 been primarily attributed to excessively strong winds. Biases with the excessively dry eastern  
233 flanks of these mountains may also be associated with the diagnostic treatment of precipitation  
234 species in CESM.

235 As further supported in Huang et al. (2016) by evaluating VR-CESM also at  $0.25^\circ$  for long-term  
236 regional climate modeling over California, it is found that VR-CESM can adequately represented  
237 regional climatological patterns with high spatial correlations. VR-CESM shows comparable per-  
238 formance as WRF at 27 km, but still overestimated overall winter precipitation (about 25%-35%)  
239 compared to reference datasets, with statistically significant difference over the western edge of  
240 the Sierra Nevada. **This bias is not alleviated by simply increasing the spatial resolution, as it still**

exists when refining this region down to 4km (Alan M. Rhoades, personal communication), suggesting that the bias might be related with more complex dynamic processes rather than treatment of the orographic effects. The spatial pattern of variability agrees well between VR-CESM and references and when assessing the frequency of strong precipitation events, VR-CESM matched closely to the UW dataset everywhere except the Central Valley.

CESM at 1 degree resolution was also assessed in order to better understand the impacts of resolution. We find that precipitation patterns over complex topography are poorly represented without capturing the spatial patterns induced by orographic effects over the Cascades and Sierra Nevada by uniform CESM at 1 degree, with total precipitation greatly underestimated, when compared to VR-CESM, gridded data and reanalysis (see the supplement). Basically, the precipitation has been smooth out at the coastal area and the mountainous regions over northwest U.S when simulated with CESM at coarse resolution. This result clearly captures the benefits of high resolution (particularly the representation of topography) in simulating precipitation features. Results are also provided for the output from a globally uniform CESM run at  $0.25^\circ$  spatial resolution with the finite volume (FV) dynamical core (Wehner et al. 2014), exhibiting comparable performance to VR-CESM (see the supplement).

We have also assessed the ENSO effect modeled by VR-CESM identified by the difference of precipitation behaviors between the warm phase (i.e. El Niño) and cool phase (i.e. La Niña) of ENSO, compared to references (see the supplement). The impact of ENSO for observational precipitation has a weaker signal compared to the VR-CESM, which might suggest that the model has an overestimation of ENSO's impact on precipitation, especially over the northwest U.S. The improvement of ENSO in the model is directly proportional to the representation of ENSO forced precipitation anomalies (AchutaRao and Sperber 2006).

264 **5. Drivers of climatological precipitation**

265 Precipitation has been observed and modeled to be changed both regionally and globally  
266 under climate warming as discussed in the introduction. The observed intensification of heavy  
267 precipitation events over the latter half of the twentieth century is attributed to the human-  
268 induced increases in GHGs over majority of Northern Hemisphere land areas (Min et al. 2011),  
269 although no significant changes in the total precipitation has been observed globally (Donat et al.  
270 2016). With the coupled effects of continued increasing CO<sub>2</sub> and SSTs in the future, precipitation  
271 is assumed to be changed driven by both the radiative changes in the lower troposphere and inten-  
272 sified water vapor evaporation over the ocean (Allen and Ingram 2002; Sugi and Yoshimura 2004).  
273 Precipitation extremes are projected to intensify continuously through the end of 21st century in  
274 both dry and wet regions with heterogeneous patterns (Donat et al. 2016).

275 As described by the Clausius-Clapeyron (C-C) equation, the water vapor content is supposed  
276 to increase by ~7% for each 1°C increase in temperature (Allan and Soden 2008). Naturally,  
277 evaporation over the ocean will increase with the climate warming, but the increasing rate may be  
278 constrained over land due to limitations by soil moisture (Cayan et al. 2010). When the air holds  
279 more water vapor, the chances of heavy rain events tend to increase even at which total precipita-  
280 tion is decreasing (Trenberth 2011), given that global total precipitation is expected to increase at  
281 a lower rate than precipitation extremes (Allan and Soden 2008). According to previous studies  
282 (e.g. (Allan and Soden 2008; O’Gorman and Schneider 2009; Min et al. 2011)), changes in more  
283 extreme precipitation follow the C-C relationship more closely than total precipitation amount  
284 (Trenberth et al. 2003). However, those changes are still remain uncertain with the increasing rate  
285 of precipitation extremes affected by multiple factors including the vertical velocity profile and  
286 temperature changes (O’Gorman and Schneider 2009).

287 The moderate or heavy precipitation events over WUS mainly result from the large-scale water  
288 flux transport from the eastern Pacific Ocean rather than directly from evaporation, usually in  
289 the form of atmospheric rivers (ARs) or orographic updraft (Trenberth et al. 2003; Neiman et al.  
290 2008). The storm track may be enhanced, which would increase ARs along the U.S. west coast  
291 with increased air water vapor content in the future (Dettinger 2011; Gao et al. 2015). In the  
292 following section, both the mean changes of precipitation and distributions of both non-extreme  
293 and extreme events are investigated as projected by the VR-CESM model under an extreme climate  
294 forcing context(i.e. RCP 8.5).

295 The precipitation of WUS has strong inter-annual variability caused by large-scale atmospheric  
296 circulation mainly associated with the ENSO (Leung et al. 2003b). As a significant driver  
297 of precipitation, ENSO modulates the storm track behavior over western U.S. with a north-  
298 west/southwest precipitation dipole (Gershunov and Barnett 1998), as discussed in 2. The pro-  
299 jected SSTs we used here states one of the possible cases of ENSO scenarios in the future. How-  
300 ever, there is still substantial uncertainty regarding how El Niño will change under global warming  
301 (Fedorov and Philander 2000; Guilyardi et al. 2009), resulting corresponding uncertainty in our  
302 results. Capotondi (2013) showed that the diversity of El Niño characteristics in CCSM4 is com-  
303 parable to what was found in observations, although, as found by Deser et al. (2012c), the overall  
304 magnitude of ENSO in CCSM4 is overestimated by 30% over the preindustrial time period.

## 305 **6. Results**

### 306 *a. Mean climatology*

307 Before proceeding with the analysis of precipitation features, it is first important to understand  
308 how the mean climatology changes in VR-CESM across time periods (Figure 4). Since the charac-

309 ter of WUS precipitation has a strong seasonal dependence, the mean climatology including mean  
310 precipitation, near-surface temperature and near-surface relative humidity are depicted in two sea-  
311 sons including the cool season (or wet season) from October to March and the warm season (or  
312 dry season) from April to September.

313 As a result of enhanced GHG concentrations, mean annual near-surface temperature ( $T2\text{avg}$ )  
314 increases by about 1.5 to 2 K from `hist` to `mid` and about 4 to 6 K from `mid` to `end`. Despite the  
315 large spatial variation in climatological temperatures, the temperature change between historical  
316 and future is fairly uniform. However, there is a slightly weaker increase in the near-coastal  
317 regions during cool season and in the lower latitude area at warm season, which might be due to  
318 the increased westerly wind during cool seasons and northward wind during warm season from  
319 the near ocean. Larger increases of temperature is also observed in warm season than cool season  
320 for about 0.5 K and 1 K for `mid` and `end` respectively.

321 Practically, whether the increase rate of the water vapor as the temperature goes up will keep the  
322 same or not will directly affect the relative humidity. As water vapor reaches saturation, conden-  
323 sation triggers clouds and precipitation. To understand the increasing rate of water vapor content  
324 under climate warming and whether relative humidity can be remain or not, 2m relative humidity  
325 (RH) is plotted in Figure 4.

326 Overall, RH remains almost the same as `hist` over the regions where temperature does not sub-  
327 stantially increase. However, in regions where temperature increase is larger than 2 K, RH is  
328 instead observed to decrease significantly relative to historical values for about 2% and 3-6%  
329 compared to `mid` and `end` respectively. In fact, trends in RH are spatially consistent with tempera-  
330 ture increase but opposite in magnitude with a spatial correlation coefficient of approximately 0.8.  
331 RH still remains the same or increase over part of the near-coastal area over the Pacific Ocean due  
332 to the lower increase of  $T2\text{avg}$  compared to the land area. This suggests that continental evapo-

333 ration and oceanic water vapor transport are insufficient to compensate for the air vapor capacity  
334 when temperature increases to certain level, which is consistent with Joshi et al. (2008), and has  
335 been observed in results by Rowell and Jones (2006) over continental and southeastern Europe  
336 and Simmons et al. (2010) over low-latitude and midlatitude land areas.

337 Based on those background changes of heat and water vapor, from hist to mid, mean precipita-  
338 tion showed a 0.2-0.6 mm/day increase during cool season with a largest change over northwest  
339 and less than 0.2 mm/day during warm season over southeast part. From hist to end, the increase is  
340 about 0.4-1.2 mm/day during cool season with also a largest change over northwest, and no notable  
341 change is observed during warm season. Nonetheless, these results are statistically significant (see  
342 Figure 5). East of the Rockies, precipitation increases through mid-century (statistically signifi-  
343 cant), but this trend appears to recede towards the end of the century (although these results are not  
344 significant). There is also a decrease of about 0.1mm/day in total precipitation over the western  
345 flank of the Sierra Nevadas during the cool season from hist to future. This decrease (about 0.15  
346 mm/day) is also found over the Cascades and the western coastal area during warm season from  
347 hist to mid. However, this decrease is not statistically significant. Majority of the precipitation  
348 over the cool season emerged from large-scale patterns, whereas warm season precipitation was  
349 from convection processes. The precipitation over WUS for moderate or heavy precipitation is  
350 mainly due to the large-scale water flux transport from the eastern Pacific Ocean rather than di-  
351 rectly from evaporation, mainly in the form of atmospheric rivers or orographic updraft (Trenberth  
352 et al. 2003; Neiman et al. 2008).

353 The increase of mean wet season precipitation over the northwest is mainly caused by the en-  
354 hanced orographic precipitation due to increased integrated vapor transport (IVT). The IVT in-  
355 creases due to higher water vapor content from increased ocean evaporation, which is affected pri-  
356 marily by climatological forcing. Over southern California, precipitation did not show significant

357 changes since no substantial increase in IVT over Eastern Pacific Ocean near southern California  
358 coast is predicted, with IVT in this region driven primarily by variations in ENSO. Since pre-  
359 cipitation over the Intermountain West during warm season is mainly results from the convection  
360 processes, precipitation is directly related with the changes of the relative humidity. As shown  
361 in Figure 4, RH has decreased over most the study area except over where the soil moisture is  
362 relatively low when going to end. Further, the changes of RH are related with the soil moisture  
363 magnitude accompanying the changes of latent heat flux during warm season.

364 According to previous studies (e.g. (Allen and Ingram 2002; Allan and Soden 2008; O’Gorman  
365 and Schneider 2009; Min et al. 2011)), changes in more extreme precipitation follow the C-C  
366 relationship more closely than total precipitation precipitation amount (Trenberth et al. 2003).  
367 In order to find out the precipitation changes in a comprehensive aspect based on our fine-scale  
368 simulations, analyses of different precipitation distributions are focused in the following part to  
369 account for the future changes of diverse precipitation events.

### 370 *b. Precipitation indices*

371 To see how precipitation changes in a comprehensive way, we have analyzed detailed precipita-  
372 tion distributions in order to account for the future changes of different precipitation events, based  
373 on our simulation results. The precipitation indices are presented in Table 1. For each index, the  
374 changes of precipitation character for each period, averaged over all ensemble members are plotted  
375 in Figure 5 (for the indices that quantify precipitation days) and Figure 6 (for the indices describing  
376 precipitation amounts). Although mean precipitation shows a weak but overall increasing trend  
377 from hist to mid and mid to end (about 10-15%), the precipitation indices exhibit substantially  
378 more unique character.

379 When comparing `hist` to `mid`, the total rainy days and frequency of non-extreme precipitation  
380 have significantly increased (about 10-15%) mainly over the central-east and southeast part of  
381 WUS, which is less obvious between `mid` and `end`. On the contrary, the frequency of non-extreme  
382 precipitation have decreased significantly over the northwest region and the eastern part of the  
383 Montana, Wyoming and Oregon from `mid` to `end` (about 10%). These changes are the primary  
384 driver for the observed change to mean precipitation exhibited in Figure 4.

385 As for extreme precipitation frequency (i.e. days with daily Pr between 10 mm and 40 mm), the  
386 number of days increases from `hist` to `mid`, but the pattern is scattered over northwest and central  
387 WUS. When comparing `mid` to `end`, there is a clear and significant increase in extreme precip-  
388 itation events over the northwest coastal area (about 20-30%) and eastern flank of the Cascades  
389 (larger than 40%). This result is consistent with Dominguez et al. (2012), who observe a robust  
390 increase in winter precipitation extremes toward the latter half of the 21st century by an ensemble  
391 of RCMs. There is a slight, but insignificant decrease over the Cascades and the Sierra Nevada  
392 (significance is low due to the high variability of precipitation). No notable predicted changes have  
393 been observed over California.

394 The associated precipitation signal under a warmer climate is more ambiguous for California  
395 (Neelin et al. 2013) considering the extreme variability on interannual time scales (Dettinger  
396 2011). Kim (2005) found that under global warming, heavy precipitation events show largest  
397 increases in the mountainous regions of the northern California Coastal Range and the Sierra  
398 Nevada. However, our results show a minor decrease (though not statistically significant) of ex-  
399 treme precipitation over the Sierra Nevada. The decrease over southwest U.S. is mainly due to the  
400 intensified La Niña in the future as shown in the Section 2.

401 For very extreme precipitation ( $\text{Pr} \geq 40 \text{ mm}$ ) events, there is an increasing trend over the north-  
402 west coast (larger than 60%) and the Cascades (about 50%) and its eastern flank (larger than 60%)

when comparing hist to end. Significant changes have also been observed over the northern mountainous part of California for about 20-40% from hist to end. The corresponding changes in rainfall amount are consistent with the changes of frequency (see Figure 6). Overall, these results indicate more extreme precipitation over the northwest U.S with changes in precipitation extremes following more consistently with the C-C relationship.

In order to understand the drivers behind the observed changes, we first examine change in moisture flux for cool seasons when WUS precipitation is primarily from water vapor influx from the Pacific Ocean (see Figure 7). We observe an increase in specific humidity at 850 hPa that accompanies the increase of the temperature in future. However, when comparing to hist, westerly wind tends to weaken in mid and end over the eastern part of the WUS and strengthen over western area.

IVT (Figure 7) for extreme precipitation days over cool seasons. Generally, IVT is useful to understand extreme precipitation events that arise from atmospheric rivers over the northwestern U.S. and from orographic uplift (especially for very extreme precipitation) (Ralph et al. 2004; Leung and Qian 2009; Dettinger 2011). Based on the observed change in IVT, it is clear that the increase in moisture influx from past to future, which is mainly due to the change of the air water vapor content with increased temperature, corresponds to the changes of precipitation extremes shown in Figure 5.

## 1) QUANTILE CORRELATION ANALYSIS

To see if changes in mean precipitation can be used to predict changes in extreme precipitation features, the correlations between Pr and specific quantiles have been calculated. Here, selected quantiles including the values at 70% (70p), 80% (80p), 90% (90p), 95% (95p) and 99% (99p) are applied based on all the daily precipitation data at each grid point within each time period.

426 These quantiles are chosen in order to account for the changes of both moderation and extreme  
427 precipitation. The mean Pr and those quantiles for hist, and the differences of these quantities  
428 among different time periods can be found in the supplemental figure. Within expectation, regions  
429 with higher Pr are associated with larger values of those quantiles, i.e. stronger precipitation  
430 extremes. This is further supported by the high correlation (about 0.7-0.9) between Pr and R20mm,  
431 R40mm, and Rxmm, not between Pr and non-extreme precipitation events.

432 Spatial correlation is assessed by computing Pearson product-moment coefficient of linear corre-  
433 lation between relevant variables. It is found that the absolute changes of Pr in future are positively  
434 related with the absolute changes of the quantiles. This relationship is at a moderate level between  
435 mid and hist (larger than 0.65), and becomes stronger when going to the end period (reaching  
436 ~0.96). Consistently, the mean Pr itself is also positively correlated with the absolute changes of  
437 the quantiles in future (around 0.5 to 0.78), except 70p between end and mid and 99p mid and  
438 hist.

439 The relative changes of quantiles are also related with the relative changes of Pr with correla-  
440 tions around 0.65 to 0.85, except 70p and 80p between end and mid. So, the area featured with  
441 higher increase of extreme precipitations in future also tends to have larger increase of its mean  
442 precipitation. However, the wetter area does not necessary have more intense changes of moder-  
443 ate and extreme precipitation than drier area. [The changes of Pr is not obviously correlated with](#)  
444 [the changes of precipitation indices, which further states that mean precipitation and precipitation](#)  
445 [events undergo different features of changing in the future.](#)

446 [might divide into four regions; PDF of each region? \[Paul: This is a good idea\]](#)

447 2) ISOLATING DIFFERENCES DUE TO CLIMATE CHANGE AND ENSO

448 The phase of ENSO is well known to have important repercussions on precipitation extremes  
449 (Larkin and Harrison 2005; Allan and Soden 2008; Maloney et al. 2014; Yoon et al. 2015). Cai  
450 et al. (2014) found a significantly increase for extraordinary precipitation along the eastern Pacific  
451 Ocean in the 21st century within the CMIP5 ensemble, associated with increasing frequency of  
452 extreme El Niño events due to greenhouse warming. In this part, we will figure out how the ENSO  
453 impacts specific regions over our study area, and whether the effects pattern will change over time.

454 ENSO from past to future, the difference of precipitation behaviors between the warm phase (i.e.  
455 El Niño) and cool phase (i.e. La Niña) of ENSO is illustrated in Figure 8 for the wet seasons of  
456 each time period. Based on the ONI index values, the mean SST anomalies are 1.38, 1.71 and 2.30  
457 K during El Niño years, and -1.16, -1.62 and -1.43 K during La Niña years for hist, mid and end  
458 respectively. The mean SSTs over the Niño 3.4 region where the are 26.83, 28.62 and 30.54°C  
459 for textsfhist, mid and end respectively. Based on the SST datasets we used here, the anomaly  
460 of ENSO has intensified. The SST anomalies of each year and each month, and their associated  
461 spatial pattern when averaged during the warm and cool phases can be found in the supplement,  
462 exhibiting the increasing frequency of El Niño during for mid and almost doubled frequency of La  
463 Niña during mid and end compared to the hist.

464 (Huang: As SSTs increase in the future, is not it normal for the anomaly of ENSO to be increased  
465 to compensate the changes of water vapor capacity? Might email Neale about this.)

466 During the El Niño phase, intensified mean precipitation is expected over the southwest (Ham-  
467 let and Lettenmaier 2007), along with reduced precipitation intensity over the northwest. In La  
468 Niña phase, the pattern is essentially reversed, with wetter conditions in the northwest and a drier  
469 situation in the Southwest. This feature is characterized as a northwest/southwest precipitation

470 dipole, triggered by ENSO's modification of the storm track (Gershunov and Barnett 1998; Le-  
471 ung et al. 2003b), along with modulation of the enhanced precipitation variability (Cayan et al.  
472 1999; Kahya and Dracup 1994). This dipole is also apparently in the frequency of rainy days and  
473 extreme precipitation events.

474 In mid and hist, ENSO is observed to intensify, which appears to be related with the changes  
475 of the strength of El Niño and La Niña. This can be explained by the SST anomaly magnitude  
476 (detrended) of warm and cold phases (see the supplement). DeFlorio et al. (2013) also found a  
477 statistically significant linkages with ENSO and PDO for both the overall and extreme intensity  
478 of wintertime precipitation over the WUS using CCSM4 (earlier form of CESM). Strengthening  
479 storm patterns associated with ENSO are also found by Maloney et al. (2014) over California using  
480 CMIP5 output under RCP8.5.

481 We have also checked the teleconnection effect of Pacific Decadal Oscillation (PDO) and it  
482 did not show strong effect alone. Precipitation features did not change notably when at the cool  
483 phase or warm phase of PDO during hist. However, together with ENSO at the same phase,  
484 PDO can have notable effect over northwest. This coupled effect has been found by previous  
485 studies Gershunov and Barnett (1998), stating ENSO and PDO can "reinforce" each other with  
486 PDO responding to the same internal atmospheric variability as ENSO (Pierce 2002). **In our**  
487 **simulations, the patterns of PDO phases differs quite a bit from past to future, though there were**  
488 **roughly an equal number of positive PDO years and negative PDO years in the data. We suppose**  
489 **that our 26 years simulation time period might not be long enough to account for the variability of**  
490 **PDO due to its duration for decades. Therefore, in this study, the PDO is not specifically analyzed.**

491 The impact of ENSO is further observed by the IVT difference over rainy days between El Niño  
492 and La Niña (see Figure 9) accompanying by the wind pattern difference at 850 hPa, showing the

493 increase of the moisture flux for the southwest and decrease for the northwest. This suggests the  
494 major role of moisture influx regulation of ENSO.

495 Based on the above results, it can be seen that the magnitude of the effects of ENSO is compara-  
496 ble or even higher than the impacts of climate forcing. For further investigation, linear regression  
497 is applied to signaling the factor effects due to ENSO and climate forcing. First, we get the SST  
498 anomaly of each cool season when ENSO mainly affect followed by the way of Niño 3.4 to be  
499 the ENSO factor values. Then, we use the GHGs values at each year to represent the climate  
500 forcing factor. The features of the precipitation indices as we defined above are used as response  
501 variables. Combined the values of all the time period and all the runs, we got the significance of  
502 these two factors' effects at each grid point based on the ANOVA (analysis of variance) output  
503 (see the supplement). Changing of the SSTs anomaly can affect most of the study area for non-  
504 extreme precipitation events, and southern regions and the Cascades and the Rocky Mountains for  
505 precipitation extremes. The GHGs factor mainly shows significant impacts over the northwest and  
506 inter-mountainous regions for both non-extreme and extreme precipitation events.

507 We have also examined the linear coefficients of these two factors over where their effects are  
508 significant to see the strength that ENSO and GHGs play at each grid point (see the supplement). It  
509 is found that the effect of the ENSO is similar to the pattern of the difference between El Niño and  
510 La Niña (see Figure 9). In contrast, the effect of the GHGs is close to the pattern of the difference  
511 between the different time periods (see Figure 5). We do acknowledge that the values might not be  
512 accurate due to the simple linear mode we used here. However, the qualitative conclusions won't  
513 change. Therefore, we assume that even the ENSO largely regulates the precipitation over different  
514 phases, it won't affect our results shown here for the changes of precipitation features from past to  
515 future. Although here is just one of the possible cases of ENSO scenarios in the future, as ENSO

516 behavior is strongly dependent on choice of climate models, the underlying principles should still  
517 be consistent.

518 Although, the strength of ENSO intensifies in the future with CESM, there is still substantial  
519 uncertainty regarding how El Niño will change under global warming as debated by plenty of  
520 studies (Fedorov and Philander 2000; Guilyardi et al. 2009), particularly as ENSO appears to be  
521 relatively insensitive to a doubling of CO<sub>2</sub> in most models (DiNezio et al. 2012). Correctly simula-  
522 tion changes to the spatial pattern of SSTs ion state-of-the-art coupled GCMs remains challenging  
523 Joseph and Nigam (2006); ?); Jha et al. (2014); Taschetto et al. (2014).

## 524 7. Discussion and Summary

525 The increased cool season precipitation extremes tend to result in higher runoff events over  
526 the northwest U.S., which are in turn associated with a greater chance of flooding and a loss of  
527 snowpack. A decrease in counts of rainy days during the warm season over central and southern  
528 California, though small in magnitude, will probably intensify the drought condition due to the  
529 deficit of soil moisture with higher evapotranspiration caused by the warmer climate in the future  
530 Cayan et al. (2010); Bell et al. (2004).

531 (Huang: Yoon et al. (2015) found a strengthened relation with ENSO for the projected increase  
532 in water cycle extremes in California using the output from CESM1 and CMIP5. Similarly by  
533 Maloney et al. (2014) using CMIP5 dataset. (check the CESM1?)

534 (Summary is to be added once the main content have been settled down The contribution of  
535 human-induced increases in greenhouse gases to the character of precipitation is confounded by  
536 patterns of variability in the atmospheric circulation. Consistent with previous studies, changes  
537 in more extreme precipitation follow the Clausius-Clapeyron relationship more closely than total  
538 precipitation amount. The changes of the strength of ENSO remains uncertain. However, the char-

539 actor of ENSO appears to be the largest factor in understanding changing precipitation extremes  
540 in the U.S. West.)

541 *Acknowledgments.* The authors would like to thank Michael Wehner for sharing the dataset and  
542 many suggestions. The authors also want to thank Alan M. Rhoades for providing the simulation  
543 output. We acknowledge the substantial efforts behind the datasets used in this study, including  
544 UW, NCDC and NARR. The simulation data used is available by request at xyhuang@ucdavis.edu.  
545 This project is supported in part by the xxx and by the xxx.

## 546 References

- 547 AchutaRao, K., and K. R. Sperber, 2006: Enso simulation in coupled ocean-atmosphere models:  
548 are the current models better? *Climate Dynamics*, **27** (1), 1–15.
- 549 Allan, R. P., and B. J. Soden, 2008: Atmospheric warming and the amplification of precipitation  
550 extremes. *Science*, **321** (5895), 1481–1484.
- 551 Allen, M. R., and W. J. Ingram, 2002: Constraints on future changes in climate and the hydrologic  
552 cycle. *Nature*, **419** (6903), 224–232.
- 553 Bell, J. L., L. C. Sloan, and M. A. Snyder, 2004: Regional changes in extreme climatic events: a  
554 future climate scenario. *Journal of Climate*, **17** (1), 81–87.
- 555 Cai, W., and Coauthors, 2014: Increasing frequency of extreme el niño events due to greenhouse  
556 warming. *Nature climate change*, **4** (2), 111–116.
- 557 Caldwell, P., 2010: California wintertime precipitation bias in regional and global climate models.  
558 *Journal of Applied Meteorology and Climatology*, **49** (10), 2147–2158.

- 559 Capotondi, A., 2013: Enso diversity in the ncar ccsm4 climate model. *Journal of Geophysical*  
560 *Research: Oceans*, **118 (10)**, 4755–4770.
- 561 Cayan, D. R., T. Das, D. W. Pierce, T. P. Barnett, M. Tyree, and A. Gershunov, 2010: Future  
562 dryness in the southwest us and the hydrology of the early 21st century drought. *Proceedings of*  
563 *the National Academy of Sciences*, **107 (50)**, 21 271–21 276.
- 564 Cayan, D. R., K. T. Redmond, and L. G. Riddle, 1999: ENSO and hydrologic extremes in the  
565 western United States\*. *Journal of Climate*, **12 (9)**, 2881–2893.
- 566 DeFlorio, M. J., D. W. Pierce, D. R. Cayan, and A. J. Miller, 2013: Western us extreme precipita-  
567 tion events and their relation to enso and pdo in ccsm4. *Journal of Climate*, **26 (12)**, 4231–4243.
- 568 Dennis, J., and Coauthors, 2011: CAM-SE: A scalable spectral element dynamical core for the  
569 Community Atmosphere Model. *International Journal of High Performance Computing Appli-*  
570 *cations*, 1094342011428142.
- 571 Deser, C., R. Knutti, S. Solomon, and A. S. Phillips, 2012a: Communication of the role of natural  
572 variability in future north american climate. *Nature Climate Change*, **2 (11)**, 775–779.
- 573 Deser, C., A. Phillips, V. Bourdette, and H. Teng, 2012b: Uncertainty in climate change projec-  
574 tions: the role of internal variability. *Climate Dynamics*, **38 (3-4)**, 527–546.
- 575 Deser, C., and Coauthors, 2012c: Enso and pacific decadal variability in the community climate  
576 system model version 4. *Journal of Climate*, **25 (8)**, 2622–2651.
- 577 Dettinger, M., 2011: Climate change, atmospheric rivers, and floods in california—a multimodel  
578 analysis of storm frequency and magnitude changes1. Wiley Online Library.

- 579 Diffenbaugh, N. S., J. S. Pal, R. J. Trapp, and F. Giorgi, 2005: Fine-scale processes regulate the  
580 response of extreme events to global climate change. *Proceedings of the National Academy of*  
581 *Sciences of the United States of America*, **102** (44), 15 774–15 778.
- 582 DiNezio, P. N., B. P. Kirtman, A. C. Clement, S.-K. Lee, G. A. Vecchi, and A. Wittenberg, 2012:  
583 Mean climate controls on the simulated response of enso to increasing greenhouse gases. *Journal*  
584 *of Climate*, **25** (21), 7399–7420.
- 585 Dominguez, F., E. Rivera, D. Lettenmaier, and C. Castro, 2012: Changes in winter precipitation  
586 extremes for the western united states under a warmer climate as simulated by regional climate  
587 models. *Geophysical Research Letters*, **39** (5).
- 588 Donat, M. G., A. L. Lowry, L. V. Alexander, P. A. OGorman, and N. Maher, 2016: More extreme  
589 precipitation in the world [rsquor] s dry and wet regions. *Nature Climate Change*.
- 590 Duffy, P., and Coauthors, 2006: Simulations of present and future climates in the western United  
591 States with four nested regional climate models. *Journal of Climate*, **19** (6), 873–895.
- 592 Duli re, V., Y. Zhang, and E. P. Salath  Jr, 2011: Extreme Precipitation and Temperature over the  
593 US Pacific Northwest: A Comparison between Observations, Reanalysis Data, and Regional  
594 Models\*. *Journal of Climate*, **24** (7), 1950–1964.
- 595 Easterling, D. R., G. A. Meehl, C. Parmesan, S. A. Changnon, T. R. Karl, and L. O. Mearns, 2000:  
596 Climate extremes: observations, modeling, and impacts. *science*, **289** (5487), 2068–2074.
- 597 Fedorov, A. V., and S. G. Philander, 2000: Is el ni o changing? *Science*, **288** (5473), 1997–2002.
- 598 Fox-Rabinovitz, M., J. C te, B. Dugas, M. D qu , and J. L. McGregor, 2006: Variable resolution  
599 general circulation models: Stretched-grid model intercomparison project (SGMIP). *Journal of*  
600 *Geophysical Research: Atmospheres (1984–2012)*, **111** (D16).

- 601 Fox-Rabinovitz, M. S., G. L. Stenchikov, M. J. Suarez, and L. L. Takacs, 1997: A finite-  
602 difference GCM dynamical core with a variable-resolution stretched grid. *Monthly weather*  
603 **review**, **125** (11), 2943–2968.
- 604 Frei, C., R. Schöll, S. Fukutome, J. Schmidli, and P. L. Vidale, 2006: Future change of precipita-  
605 tion extremes in Europe: Intercomparison of scenarios from regional climate models. *Journal*  
606 *of Geophysical Research: Atmospheres (1984–2012)*, **111** (D6).
- 607 Gao, Y., J. Lu, L. R. Leung, Q. Yang, S. Hagos, and Y. Qian, 2015: Dynamical and thermodynami-  
608 cal modulations on future changes of landfalling atmospheric rivers over western north america.  
609 *Geophysical Research Letters*, **42** (17), 7179–7186.
- 610 Gates, W. L., 1992: AMIP: The Atmospheric Model Intercomparison Project. *Bulletin of the*  
611 *American Meteorological Society*, **73**, 1962–1970.
- 612 Gershunov, A., and T. P. Barnett, 1998: Interdecadal modulation of enso teleconnections. *Bulletin*  
613 *of the American Meteorological Society*, **79** (12), 2715–2725.
- 614 Grodsky, S. A., J. A. Carton, S. Nigam, and Y. M. Okumura, 2012: Tropical atlantic biases in  
615 ccesm4. *Journal of Climate*, **25** (11), 3684–3701.
- 616 Guilyardi, E., A. Wittenberg, A. Fedorov, M. Collins, C. Wang, A. Capotondi, G. J. Van Olden-  
617 borgh, and T. Stockdale, 2009: Understanding el niño in ocean-atmosphere general circulation  
618 models. *Bulletin of the American Meteorological Society*, **90** (3), 325.
- 619 Hamlet, A. F., and D. P. Lettenmaier, 2005: Production of Temporally Consistent Gridded Precipi-  
620 tation and Temperature Fields for the Continental United States\*. *Journal of Hydrometeorology*,  
621 **6** (3), 330–336.

- 622 Hamlet, A. F., and D. P. Lettenmaier, 2007: Effects of 20th century warming and climate variability  
623 on flood risk in the western us. *Water Resources Research*, **43** (6).
- 624 Hegerl, G. C., F. W. Zwiers, P. A. Stott, and V. V. Kharin, 2004: Detectability of anthropogenic  
625 changes in annual temperature and precipitation extremes. *Journal of Climate*, **17** (19), 3683–  
626 3700.
- 627 Huang, X., A. M. Rhoades, P. A. Ullrich, and C. M. Zarzycki, 2016: An evaluation of the vari-  
628 able resolution-cesm for modeling california's climate. *Journal of Advances in Modeling Earth*  
629 *Systems*.
- 630 Huang, X., and P. A. Ullrich, 2016: Irrigation impacts on california's climate with the variable-  
631 resolution cesm. *Journal of Advances in Modeling Earth Systems*.
- 632 Hurrell, J. W., J. J. Hack, D. Shea, J. M. Caron, and J. Rosinski, 2008: A new sea surface temper-  
633 ature and sea ice boundary dataset for the Community Atmosphere Model. *Journal of Climate*,  
634 **21** (19), 5145–5153.
- 635 Hurrell, J. W., and Coauthors, 2013: The community earth system model: A framework for col-  
636 laborative research. *Bulletin of the American Meteorological Society*, **94** (9), 1339–1360.
- 637 Jha, B., Z.-Z. Hu, and A. Kumar, 2014: Sst and enso variability and change simulated in historical  
638 experiments of cmip5 models. *Climate dynamics*, **42** (7-8), 2113–2124.
- 639 Joseph, R., and S. Nigam, 2006: Enso evolution and teleconnections in ipcc's twentieth-century  
640 climate simulations: Realistic representation? *Journal of Climate*, **19** (17), 4360–4377.
- 641 Joshi, M. M., J. M. Gregory, M. J. Webb, D. M. Sexton, and T. C. Johns, 2008: Mechanisms for  
642 the land/sea warming contrast exhibited by simulations of climate change. *Climate Dynamics*,  
643 **30** (5), 455–465.

- 644 Kahya, E., and J. A. Dracup, 1994: The influences of type 1 el nino and la nina events on stream-  
flows in the pacific southwest of the united states. *Journal of Climate*, **7 (6)**, 965–976.
- 645
- 646 Kao, H.-Y., and J.-Y. Yu, 2009: Contrasting eastern-pacific and central-pacific types of enso.  
647 *Journal of Climate*, **22 (3)**, 615–632.
- 648
- 649 Karl, T. R., N. Nicholls, and A. Ghazi, 1999: Clivar/gcos/wmo workshop on indices and indicators  
for climate extremes workshop summary. *Weather and Climate Extremes*, Springer, 3–7.
- 650
- 651 Kharin, V. V., F. W. Zwiers, X. Zhang, and G. C. Hegerl, 2007: Changes in temperature and  
precipitation extremes in the IPCC ensemble of global coupled model simulations. *Journal of*  
652 *Climate*, **20 (8)**, 1419–1444.
- 653
- 654 Kim, J., 2005: A projection of the effects of the climate change induced by increased co2 on  
extreme hydrologic events in the western us. *Climatic Change*, **68 (1-2)**, 153–168.
- 655
- 656 Laprise, R., and Coauthors, 2008: Challenging some tenets of regional climate modelling. *Meteo-*  
*rology and Atmospheric Physics*, **100 (1-4)**, 3–22.
- 657
- 658 Larkin, N. K., and D. Harrison, 2005: On the definition of el niño and associated seasonal average  
us weather anomalies. *Geophysical Research Letters*, **32 (13)**.
- 659
- 660 Leung, L. R., L. O. Mearns, F. Giorgi, and R. L. Wilby, 2003a: Regional climate research: needs  
and opportunities. *Bulletin of the American Meteorological Society*, **84 (1)**, 89–95.
- 661
- 662 Leung, L. R., and Y. Qian, 2009: Atmospheric rivers induced heavy precipitation and flooding in  
the western US simulated by the WRF regional climate model. *Geophysical research letters*,  
663 **36 (3)**.

- 664 Leung, L. R., Y. Qian, and X. Bian, 2003b: Hydroclimate of the western United States based on  
665 observations and regional climate simulation of 1981-2000. Part I: Seasonal statistics. *Journal*  
666 *of Climate*, **16 (12)**, 1892–1911.
- 667 Maloney, E. D., and Coauthors, 2014: North american climate in cmip5 experiments: part iii:  
668 assessment of twenty-first-century projections\*. *Journal of Climate*, **27 (6)**, 2230–2270.
- 669 Maurer, E., A. Wood, J. Adam, D. Lettenmaier, and B. Nijssen, 2002: A long-term hydrologically  
670 based dataset of land surface fluxes and states for the conterminous United States\*. *Journal of*  
671 *climate*, **15 (22)**, 3237–3251.
- 672 McDonald, A., 2003: Transparent boundary conditions for the shallow-water equations: testing in  
673 a nested environment. *Monthly weather review*, **131 (4)**, 698–705.
- 674 Meehl, G. A., H. Teng, and G. Bannister, 2006: Future changes of el niño in two global coupled  
675 climate models. *Climate Dynamics*, **26 (6)**, 549–566.
- 676 Mesinger, F., and K. Veljovic, 2013: Limited area NWP and regional climate modeling: a test  
677 of the relaxation vs Eta lateral boundary conditions. *Meteorology and Atmospheric Physics*,  
678 **119 (1-2)**, 1–16.
- 679 Mesinger, F., and Coauthors, 2006: North American regional reanalysis. *Bulletin of the American*  
680 *Meteorological Society*, **87**, 343–360.
- 681 Min, S.-K., X. Zhang, F. W. Zwiers, and G. C. Hegerl, 2011: Human contribution to more-intense  
682 precipitation extremes. *Nature*, **470 (7334)**, 378–381.
- 683 Neale, R. B., and Coauthors, 2010a: Description of the NCAR community atmosphere model  
684 (CAM 5.0). *NCAR Tech. Note NCAR/TN-486+ STR*.

- 685 Neale, R. B., and Coauthors, 2010b: Description of the NCAR Community Atmosphere Model  
686 (CAM 5.0). NCAR Technical Note NCAR/TN-486+STR, National Center for Atmospheric Re-  
687 search, Boulder, Colorado, 268 pp.
- 688 Neelin, J. D., B. Langenbrunner, J. E. Meyerson, A. Hall, and N. Berg, 2013: California winter  
689 precipitation change under global warming in the coupled model intercomparison project phase  
690 5 ensemble. *Journal of Climate*, **26** (17), 6238–6256.
- 691 Neiman, P. J., F. M. Ralph, G. A. Wick, J. D. Lundquist, and M. D. Dettinger, 2008: Meteorolog-  
692 ical characteristics and overland precipitation impacts of atmospheric rivers affecting the west  
693 coast of north america based on eight years of ssm/i satellite observations. *Journal of Hydrom-  
694 eteorology*, **9** (1), 22–47.
- 695 NOAA, 2013: Defining El Niño and La Niña. Accessed: 2015-  
696 08-20, [https://www.climate.gov/news-features/understanding-climate/  
697 watching-el-nio-and-la-nia-noaa-adapts-global-warming](https://www.climate.gov/news-features/understanding-climate/watching-el-nio-and-la-nia-noaa-adapts-global-warming).
- 698 O’Gorman, P. A., and T. Schneider, 2009: The physical basis for increases in precipitation ex-  
699 tremes in simulations of 21st-century climate change. *Proceedings of the National Academy of  
700 Sciences*, **106** (35), 14 773–14 777.
- 701 Oleson, K., and Coauthors, 2010: Technical description of version 4.0 of the Community Land  
702 Model (CLM). NCAR Technical Note NCAR/TN-478+STR, National Center for Atmospheric  
703 Research, Boulder, Colorado, 257 pp. doi:10.5065/D6FB50WZ.
- 704 Pierce, D. W., 2002: The role of sea surface temperatures in interactions between enso and the  
705 north pacific oscillation. *Journal of climate*, **15** (11), 1295–1308.

- 706 Ralph, F. M., P. J. Neiman, and G. A. Wick, 2004: Satellite and caljet aircraft observations of  
707 atmospheric rivers over the eastern north pacific ocean during the winter of 1997/98. *Monthly*  
708 *Weather Review*, **132** (7), 1721–1745.
- 709 Rauscher, S. A., E. Coppola, C. Piani, and F. Giorgi, 2010: Resolution effects on regional climate  
710 model simulations of seasonal precipitation over Europe. *Climate dynamics*, **35** (4), 685–711.
- 711 Rauscher, S. A., T. D. Ringler, W. C. Skamarock, and A. A. Mirin, 2013: Exploring a Global  
712 Multiresolution Modeling Approach Using Aquaplanet Simulations. *Journal of Climate*, **26** (8),  
713 2432–2452.
- 714 Rhoades, A. M., X. Huang, P. A. Ullrich, and C. M. Zarzycki, 2015: Characterizing Sierra Nevada  
715 snowpack using variable-resolution CESM. *Journal of Applied Meteorology and Climatology*,  
716 (2015).
- 717 Riahi, K., and Coauthors, 2011: RCP 8.5A scenario of comparatively high greenhouse gas emis-  
718 sions. *Climatic Change*, **109** (1-2), 33–57.
- 719 Rowell, D. P., and R. G. Jones, 2006: Causes and uncertainty of future summer drying over europe.  
720 *Climate Dynamics*, **27** (2-3), 281–299.
- 721 Salathé Jr, E. P., R. Steed, C. F. Mass, and P. H. Zahn, 2008: A High-Resolution Climate Model  
722 for the US Pacific Northwest: Mesoscale Feedbacks and Local Responses to Climate Change\*.  
723 *Journal of Climate*, **21** (21), 5708–5726.
- 724 Scoccimarro, E., M. Zampieri, A. Bellucci, A. Navarra, and Coauthors, 2013: Heavy precipitation  
725 events in a warmer climate: results from CMIP5 models. *Journal of climate*.

- 726 Seneviratne, S. I., and Coauthors, 2012: Changes in climate extremes and their impacts on the  
727 natural physical environment. *Managing the risks of extreme events and disasters to advance*  
728 *climate change adaptation*, 109–230.
- 729 Sillmann, J., V. Kharin, F. Zwiers, X. Zhang, and D. Bronaugh, 2013: Climate extremes indices  
730 in the cmip5 multimodel ensemble: Part 2. future climate projections. *Journal of Geophysical*  
731 *Research: Atmospheres*, **118 (6)**, 2473–2493.
- 732 Simmons, A., K. Willett, P. Jones, P. Thorne, and D. Dee, 2010: Low-frequency variations  
733 in surface atmospheric humidity, temperature, and precipitation: Inferences from reanalyses  
734 and monthly gridded observational data sets. *Journal of Geophysical Research: Atmospheres*,  
735 **115 (D1)**.
- 736 Singh, D., M. Tsiang, B. Rajaratnam, and N. S. Diffenbaugh, 2013: Precipitation extremes over the  
737 continental United States in a transient, high-resolution, ensemble climate model experiment.  
738 *Journal of Geophysical Research: Atmospheres*, **118 (13)**, 7063–7086.
- 739 Small, R. J., and Coauthors, 2014: A new synoptic scale resolving global climate simulation using  
740 the community earth system model. *Journal of Advances in Modeling Earth Systems*, **6 (4)**,  
741 1065–1094.
- 742 Staniforth, A. N., and H. L. Mitchell, 1978: A variable-resolution finite-element technique for  
743 regional forecasting with the primitive equations. *Monthly Weather Review*, **106 (4)**, 439–447.
- 744 Sugi, M., and J. Yoshimura, 2004: A mechanism of tropical precipitation change due to co2  
745 increase. *Journal of climate*, **17 (1)**, 238–243.

- 746 Taschetto, A. S., A. S. Gupta, N. C. Jourdain, A. Santoso, C. C. Ummenhofer, and M. H. England,  
747 2014: Cold tongue and warm pool enso events in cmip5: mean state and future projections.  
748 *Journal of Climate*, **27 (8)**, 2861–2885.
- 749 Taylor, M. A., 2011: Conservation of mass and energy for the moist atmospheric primitive equa-  
750 tions on unstructured grids. *Numerical Techniques for Global Atmospheric Models*, Springer,  
751 357–380.
- 752 Tebaldi, C., K. Hayhoe, J. M. Arblaster, and G. A. Meehl, 2006: Going to the extremes. *Climatic  
753 change*, **79 (3-4)**, 185–211.
- 754 Trenberth, K. E., 2011: Changes in precipitation with climate change. *Climate Research*, **47 (1)**,  
755 123.
- 756 Trenberth, K. E., A. Dai, R. M. Rasmussen, and D. B. Parsons, 2003: The changing character of  
757 precipitation. *Bulletin of the American Meteorological Society*, **84 (9)**, 1205–1217.
- 758 Walker, M. D., and N. S. Diffenbaugh, 2009: Evaluation of high-resolution simulations of daily-  
759 scale temperature and precipitation over the united states. *Climate dynamics*, **33 (7-8)**, 1131–  
760 1147.
- 761 Wehner, M. F., 2013: Very extreme seasonal precipitation in the NARCCAP ensemble: model  
762 performance and projections. *Climate Dynamics*, **40 (1-2)**, 59–80.
- 763 Wehner, M. F., R. L. Smith, G. Bala, and P. Duffy, 2010: The effect of horizontal resolution  
764 on simulation of very extreme US precipitation events in a global atmosphere model. *Climate  
765 dynamics*, **34 (2-3)**, 241–247.

- 766 Wehner, M. F., and Coauthors, 2014: The effect of horizontal resolution on simulation qual-  
767 ity in the Community Atmospheric Model, CAM5.1. *J. Model. Earth. Sys.*, doi:10.1002/  
768 2013MS000276.
- 769 Yoon, J.-H., S. S. Wang, R. R. Gillies, B. Kravitz, L. Hipps, and P. J. Rasch, 2015: Increasing  
770 water cycle extremes in California and in relation to ENSO cycle under global warming. *Nature*  
771 *communications*, **6**.
- 772 Zarzycki, C. M., C. Jablonowski, and M. A. Taylor, 2014: Using Variable-Resolution Meshes  
773 to Model Tropical Cyclones in the Community Atmosphere Model. *Monthly Weather Review*,  
774 **142** (3), 1221–1239.
- 775 Zarzycki, C. M., C. Jablonowski, D. R. Thatcher, and M. A. Taylor, 2015: Effects of localized grid  
776 refinement on the general circulation and climatology in the Community Atmosphere Model.  
777 *Journal of Climate*, **(2015)**.
- 778 Zhang, X., L. Alexander, G. C. Hegerl, P. Jones, A. K. Tank, T. C. Peterson, B. Trewin, and  
779 F. W. Zwiers, 2011: Indices for monitoring changes in extremes based on daily temperature and  
780 precipitation data. *Wiley Interdisciplinary Reviews: Climate Change*, **2** (6), 851–870.
- 781 Zhang, X., J. Wang, F. W. Zwiers, and P. Y. Groisman, 2010: The influence of large-scale climate  
782 variability on winter maximum daily precipitation over North America. *Journal of Climate*,  
783 **23** (11), 2902–2915.
- 784 update the mesh grid plot
- 785 update the plot with new label levels

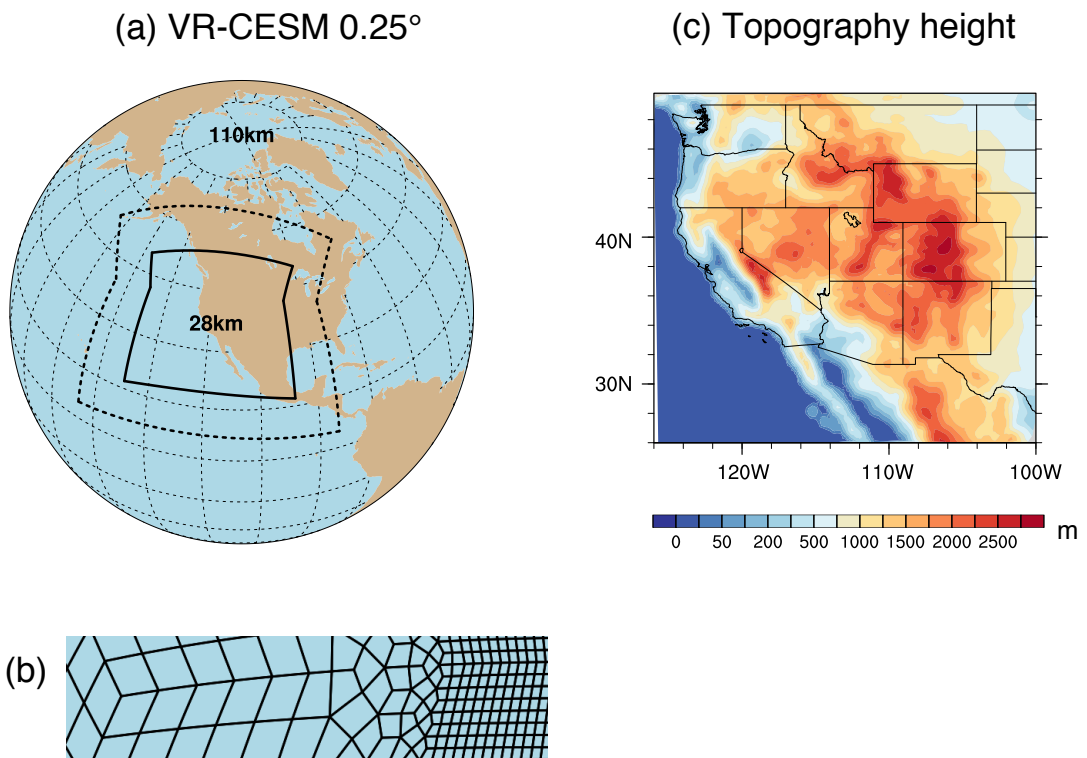
786 LIST OF TABLES

TABLE 1. Precipitation indices employed in this study.

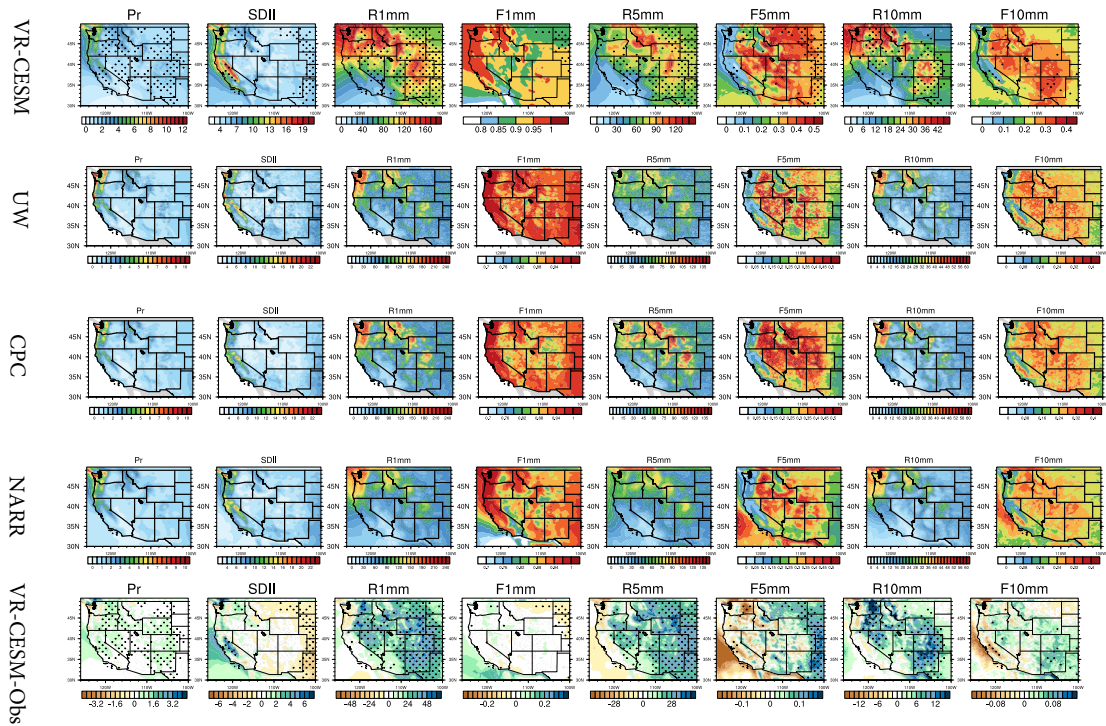
Name	Definition
Pr	Mean daily precipitation
R1mm	Number of days per year with Pr>1 mm
SDII	Simple precipitation intensity index: Precipitation amount / $\langle R1mm \rangle$ (mm/day)
R5mm	Number of days per year with Pr>1 mm and Pr=<5 mm
R10mm	Number of days per year with Pr>5 mm and Pr=<10 mm
R20mm	Number of days per year with Pr>10 mm and Pr=<20 mm
R40mm	Number of days per year with Pr>20 mm and Pr=<40 mm
Rxmm	Number of days per year with Pr>40 mm
F1mm	Fraction of precipitation contributed to the total precipitation for days of R1mm (similarly for F5mm, F10mm, F20mm, F40mm and Fxmm)
P5mm	Precipitation amount from R5mm (similarly for P10mm, P20mm, F40mm, Pxmm)

788 **LIST OF FIGURES**

789 <b>Fig. 1.</b>	(a) The approximate grid spacing used for the VR-CESM $0.25^\circ$ mesh. (b) A depiction of 790 the transition from the global $1^\circ$ resolution mesh through two layers of refinement to $0.25^\circ$ . 791 (c) Topography height over the study area. . . . .	41
792 <b>Fig. 2.</b>	Mean precipitation and other related indices from VR-CESM and reference datasets over 793 1980-2005. (Note: Grids with statistically significance difference are marked with stip- 794 pling.) . . . . .	42
795 <b>Fig. 3.</b>	The mean precipitation and other related indices from VR-CESM and reference datasets 796 over 1980-2005 (continued). . . . .	43
797 <b>Fig. 4.</b>	The mean precipitation ( $Pr$ ), 2m average temperature ( $T2avg$ ), and 2m relative humidity 798 ( $RH$ ) averaged over each time period. (Note: Grids with statistically significance difference 799 for the $RH$ are marked with stippling.) . . . . .	44
800 <b>Fig. 5.</b>	Differences of precipitation behaviors from past to future over WUS averaged of each time 801 period. (Note: Grids with statistically significance difference are marked with stippling.) . . . . .	45
802 <b>Fig. 6.</b>	Differences of precipitation behaviors from past to future over WUS averaged of each time 803 period (continued). . . . .	46
804 <b>Fig. 7.</b>	Changes of specific humidity and horizontal wind pattern at 850hPa for moisture flux il- 805 lustration, and IVT for simulations under different time period of wet season (October to 806 March). (Note: The minimum wind vector is set to be 0.5 m/s, therefore, the wind less than 807 0.5 m/s is also plotted at the minimum length for better visualization.) <b>For all difference</b> 808 <b>plots, make sure to use a common [min,max] range as its currently difficult to tease out dif-</b> 809 <b>ferences. Difference plots should also use a different color table to the mean results (perhaps</b> 810 <b>a single color color table?).</b> . . . . .	47
811 <b>Fig. 8.</b>	Difference of precipitation behaviors between warm and cool phases of ENSO from past to 812 future over WUS averaged of each time period. . . . .	48
813 <b>Fig. 9.</b>	Changes of IVT for simulations under different phases of ENSO of wet season (October to 814 March). (Note: The minimum wind vector is set to be 0.5 m/s, therefore, the wind less than 815 0.5 m/s is also plotted at the minimum length for better visualization.) . . . . .	49

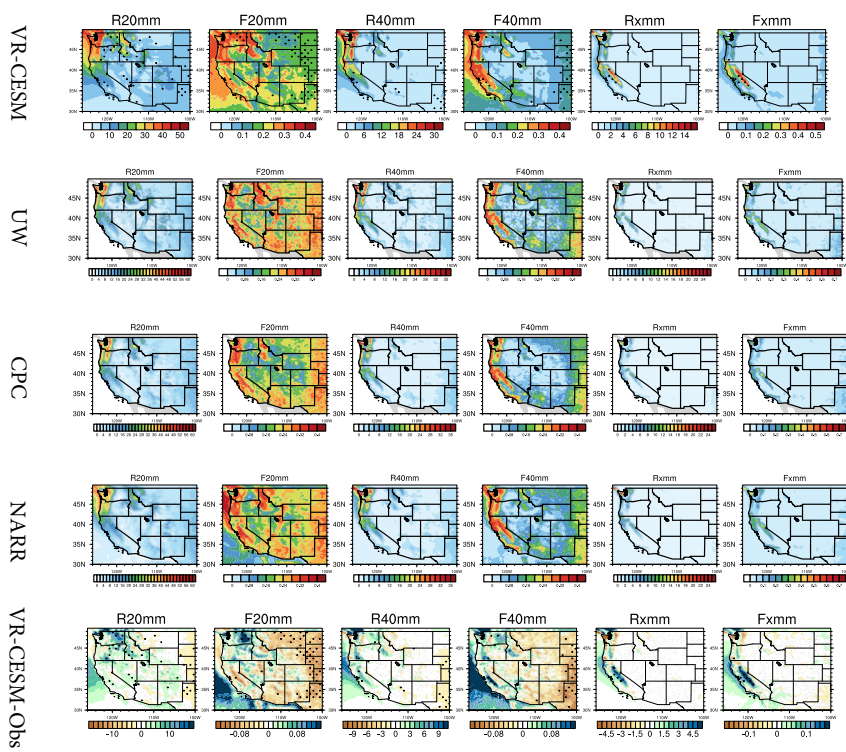


816 FIG. 1. (a) The approximate grid spacing used for the VR-CESM  $0.25^\circ$  mesh. (b) A depiction of the transition  
 817 from the global  $1^\circ$  resolution mesh through two layers of refinement to  $0.25^\circ$ . (c) Topography height over the  
 818 study area.

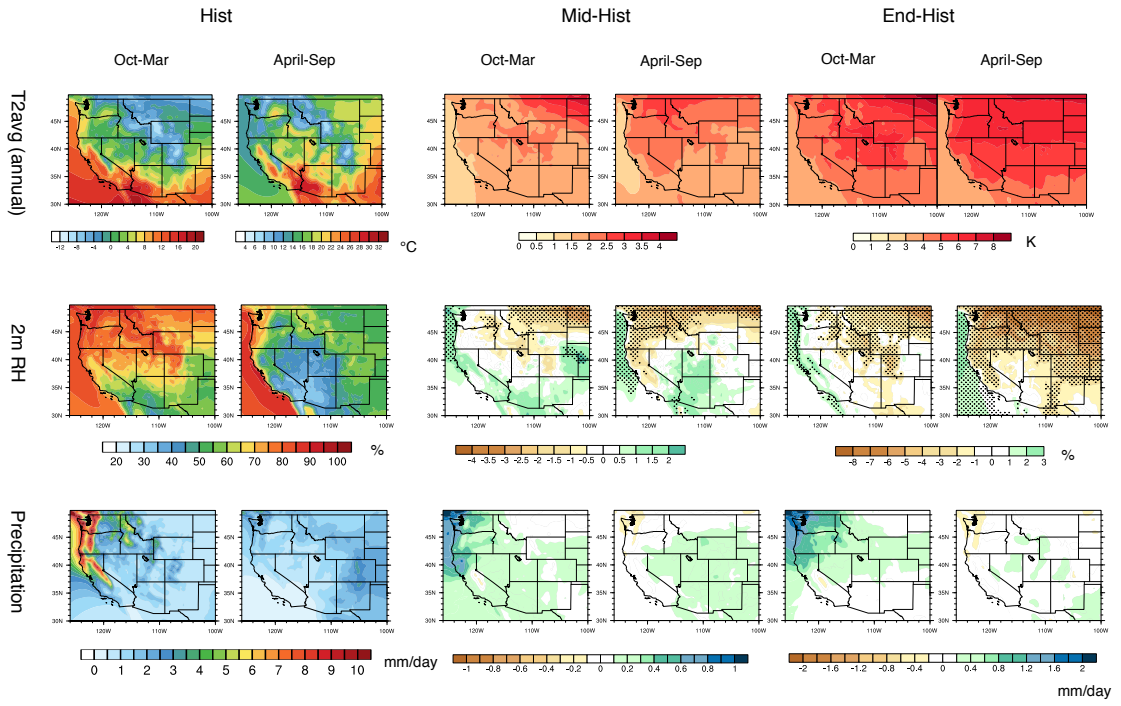


819 FIG. 2. Mean precipitation and other related indices from VR-CESM and reference datasets over 1980-2005.

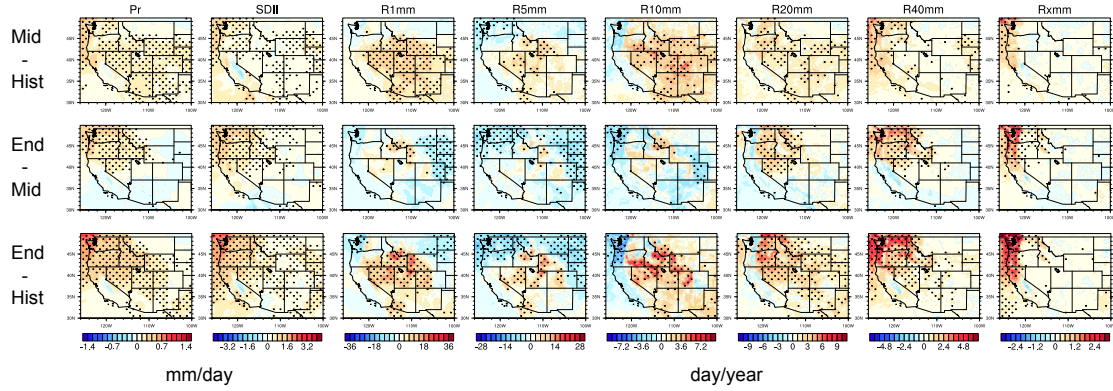
820 (Note: Grids with statistically significant difference are marked with stippling.)



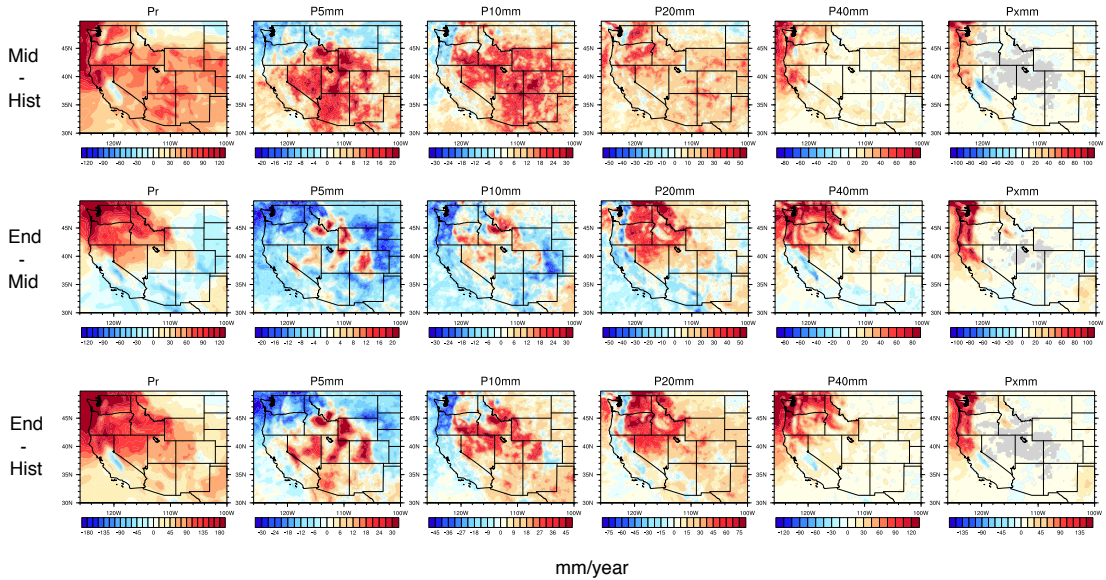
821 FIG. 3. The mean precipitation and other related indices from VR-CESM and reference datasets over 1980-  
 822 2005 (continued).



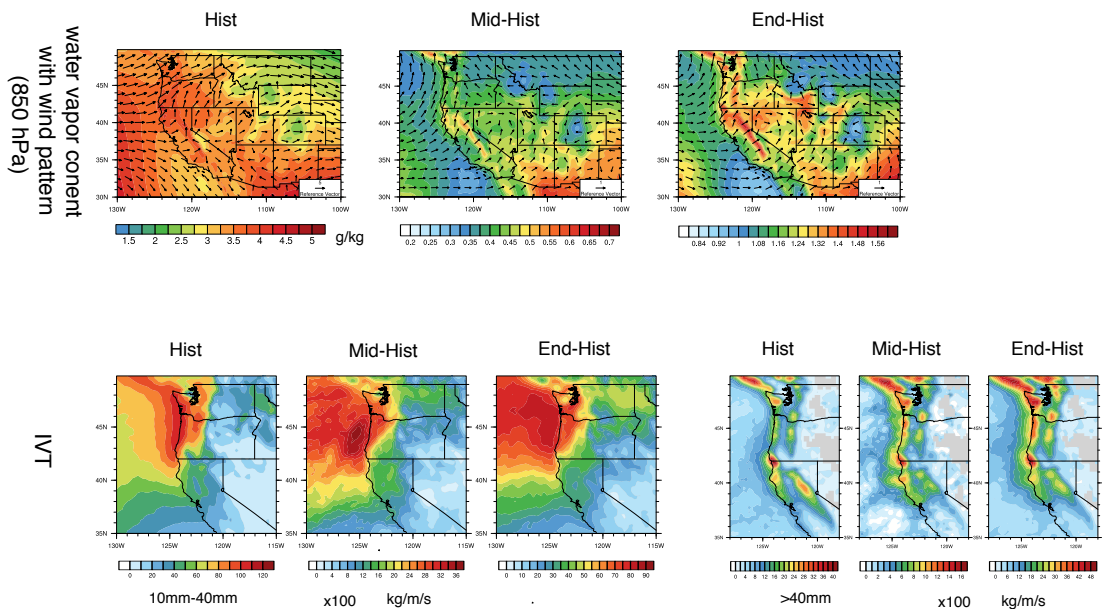
823 FIG. 4. The mean precipitation (Pr), 2m average temperature (T2avg), and 2m relative humidity (RH) aver-  
 824 aged over each time period. (Note: Grids with statistically significance difference for the RH are marked with  
 825 stippling.)



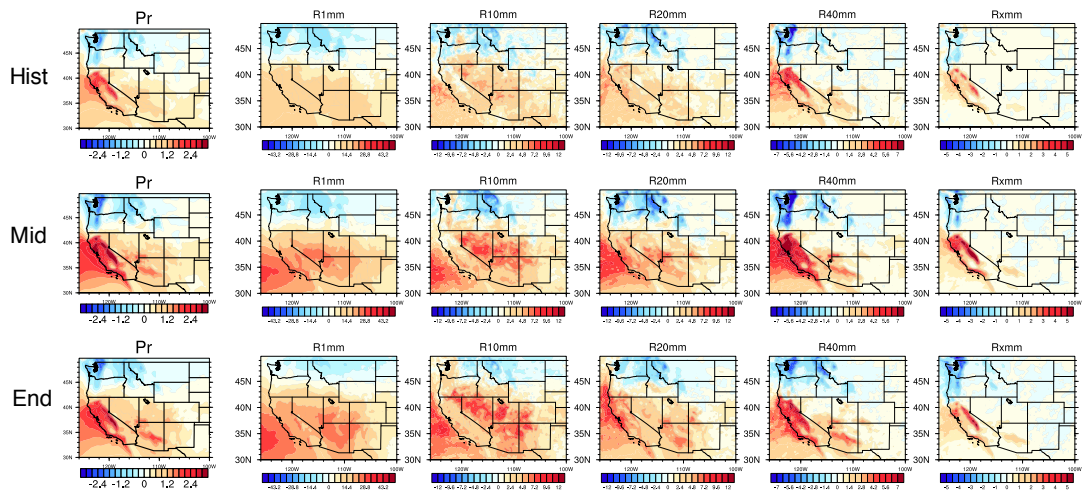
826 FIG. 5. Differences of precipitation behaviors from past to future over WUS averaged of each time period.  
 827 (Note: Grids with statistically significance difference are marked with stippling.)



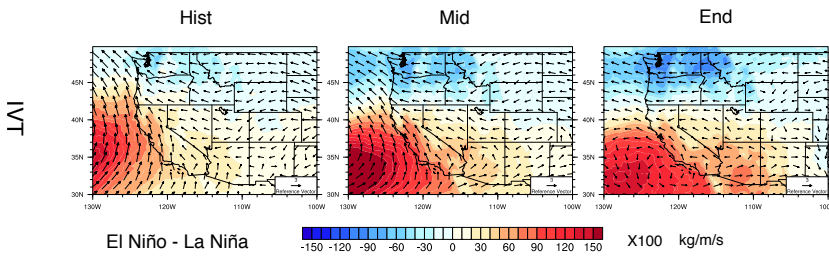
828 FIG. 6. Differences of precipitation behaviors from past to future over WUS averaged of each time period  
 829 (continued).



830 FIG. 7. Changes of specific humidity and horizontal wind pattern at 850hPa for moisture flux illustration, and  
 831 IVT for simulations under different time period of wet season (October to March). (Note: The minimum wind  
 832 vector is set to be 0.5 m/s, therefore, the wind less than 0.5 m/s is also plotted at the minimum length for better  
 833 visualization.) For all difference plots, make sure to use a common [min,max] range as its currently difficult  
 834 to tease out differences. Difference plots should also use a different color table to the mean results (perhaps a  
 835 single color color table?).



836 FIG. 8. Difference of precipitation behaviors between warm and cool phases of ENSO from past to future  
 837 over WUS averaged of each time period.



838 FIG. 9. Changes of IVT for simulations under different phases of ENSO of wet season (October to March).  
 839 (Note: The minimum wind vector is set to be 0.5 m/s, therefore, the wind less than 0.5 m/s is also plotted at the  
 840 minimum length for better visualization.)